ACS APPLIED MATERIALS & INTERFACES

Research Article

www.acsami.org

Enhanced Stability of Aluminum Nanoparticle-Doped Organic Solar Cells

Maria Sygletou,[†,‡,∥] George Kakavelakis,[†,⊥] Barbara Paci,[*,§] Amanda Generosi,[§] Emmanuel Kymakis,[†] and Emmanuel Stratakis[*,†,‡,⊥]

[†]Center of Materials Technology and Photonics & Electrical Engineering Department, Technological Educational Institute (TEI) of Crete, Heraklion 71004, Crete, Greece

[‡]Institute of Electronic Structure and Laser, Foundation for Research and Technology - Hellas, P.O. Box 1527, Heraklion 71110, Crete, Greece

[∥]Department of Physics, University of Crete, Heraklion, 71003, Crete, Greece

[§]CNR - Istituto di Struttura della Materia, Area di Ricerca di Tor Vergata, Via del fosso del cavaliere, 100, 00133, Rome, Italy

[⊥]Department of Materials Science and Technology, University of Crete, Heraklion, 71003, Crete, Greece

Supporting Information

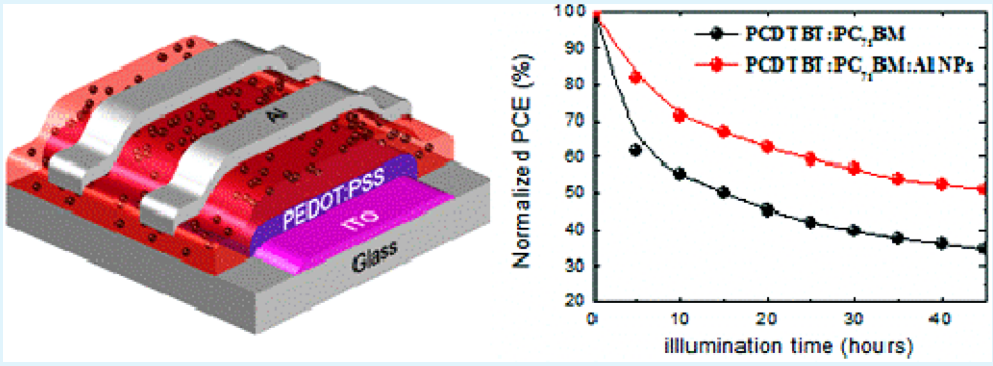

ABSTRACT: Enhancement of the stability of bulk heterojunction (BHJ) organic photovoltaic (OPV) devices is reported by the addition of surfactant-free aluminum (Al) nanoparticles (NPs) into the photoactive layer. The universality of the effect is demonstrated for two different BHJ systems, namely, the well-studied poly(3-hexylthiophene-2,5-diyl):phenyl-C61-butyric acid methyl ester (P3HT:PCBM) as well as the high efficient poly[*N*-9′-heptadecanyl-2,7-carbazole-*alt*-5,5-(4′,7′-di-2-thienyl-2′,1′,3′-benzothiadiazole)]:[6,6]-phenyl-C71-butyric acid methyl ester (PCDTBT:$PC_{71}BM$). It is shown that the lifetime of the devices with Al NPs, operating under continuous one-sun illumination in ambient conditions, is more than three times longer compared to the reference devices. Using complementary analytical techniques for in situ studies, we have explored the underlying mechanisms behind the observed stability improvement in the case of the P3HT:PCBM system. In particular, laser-induced fluorescence (LIF), photoluminescence decay and Fourier transform infrared (FTIR) spectroscopy experiments were performed and complemented with device degradation electrical measurements. It is found that the embedded Al NPs act as performance stabilizers, giving rise to enhanced structural stability of the active blend. Furthermore, it is revealed that the observed improvement can also be ascribed to NP-mediated mitigation of the photo-oxidation effect. This study addresses a major issue in OPV devices, that is, photoinduced stability, indicating that the exploitation of Al NPs could be a successful approach toward fabricating OPVs exhibiting long-term operating lifetimes.

KEYWORDS: *organic photovoltaics, bulk heterojunction, aluminum nanoparticles, degradation mechanisms, stability, in situ characterization methods*

1. INTRODUCTION

Organic semiconducting materials exhibit large potential for photovoltaic energy conversion. The major attention on organic photovoltaics (OPVs) originates from the fact that organic compounds are of much lower cost than silicon or any of the other PV materials available to date, as well as the fact that they can be fabricated using low temperature solution processed techniques. Recently, notable efficiency improvements have been obtained. For instance, using bulk heterojunction (BHJ) OPV devices, power conversion efficiencies (PCE) exceeding 9% were reported[1,2] for single junction and up to 11% for multijunction tandem solar cells.[3]

Received: May 8, 2015
Accepted: July 29, 2015
Published: July 29, 2015

DOI: 10.1021/acsami.5b03970
ACS Appl. Mater. Interfaces 2015, 7, 17756−17764

Nonetheless, further reasearch effort toward increasing PCE as well as improving device lifetime is required. Here, we focus on OPV devices incorporating metallic nanoparticles (NPs) into the active layer of OPV cells because such systems have been demonstrated to be a very promising strategy for enhancing OPV performances[4,5] due to localized surface plasmon resonance (LSPR)[6−8] or multiple LSPR effects,[9] light scattering,[10,11] multiple light scattering effects,[12] the synergy of these effects,[13,14] the plasmonic effects of metal NP clusters,[15] or the utilization of multiple metal NPs,[16] as well as the BHJ blend structure improvement.[17] Conversely, as OPV efficiencies steadily improve, the investigation of performance degradation consequent to solar irradiation and outdoor operation becomes increasingly important and remains a major issue that needs to be addressed for OPV commercialization.[18] Indeed, it has been shown that the light-induced instability of BHJ OPV cells is directed by complex photodegradation pathways related to the structural, morphological, and interfacial properties of virtually any layer and interface of OPV devices.[18−21] In this context, complementary physicochemical characterization techniques are required for a complete understanding of the effect of each of the parameters involved and realization of OPV devices exhibiting improved stability.

In this work, we report a new strategy to enhance the durability of BHJ OPV devices via the addition of highly stable surfactant-free Al NPs into the photoactive layer. The improved stability was demonstrated for two different BHJ systems, namely, poly(3-hexylthiophene-2,5-diyl):phenyl-C61-butyric acid methyl ester (P3HT:PCBM) and poly[*N*-9′-heptadecanyl-2,7-carbazole-*alt*-5,5-(4′,7′-di-2-thienyl-2′,1′,3′-benzothiadiazole)]:[6,6]-phenyl-C71-butyric acid methyl ester (PCDTBT:$PC_{71}BM$), and the underlying degradation mechanisms were explored by optical spectroscopy techniques complemented with device degradation electrical measurements. We postulate that the effect of Al NPs is 2-fold: on one hand, as previously reported, they give rise to enhanced structural stability of the active layer components,[17] whereas on the other hand, they lead to significant mitigation of the photooxidation effect. Although, the scope of this paper is limited to exploring degradation processes in the Al NP-doped P3HT:PCBM active layer, our findings are further supported by improvement in the durability of high-efficiency Al NP-doped PCDTBT:$PC_{71}BM$ OPV devices as well.

2. EXPERIMENTAL SECTION

2.1. NP Generation. Details on the generation procedure of Al NPs have already been reported elsewhere.[22] The generation of metal NPs was performed by ultrafast (femtosecond or picosecond) laser ablation of metallic targets (99.99%). The targets were placed into a Pyrex cell and completely covered by a layer of absolute ethanol. A femtosecond laser beam (wavelength of 800 nm, pulse duration of ∼100 fs, and repetition rate of 1 kHz) was focused onto the target. The cell was mounted on a stage and continuously rotated during laser exposure. Laser irradiation gives rise to a high temperature gradient in the metal bulk and melts a thin layer of the target. A fraction of the molten layer of the target is dispersed into the liquid in the form of NPs. As prepared, Al NPs were spherical and had relatively uniform diameters. The respective size distribution determined from a series of TEM images (Figure S1) indicates that the majority of NPs exhibit sizes ranging from 10 to 70 nm with an average of ∼30 nm.

2.2. TiO_x Solution Preparation. Titanium(IV) isopropoxide ($Ti[OCH(CH_3)_2]_4$, 5 mL), 2-methoxyethanol ($CH_3OCH_2CH_2OH$, 20 mL), and ethanolamine ($H_2NCH_2CH_2OH$, 2 mL) were added to a three-necked flask under nitrogen atmosphere. The solution was then stirred for 1 h at room temperature, followed by heating at 80 °C for 1h and 120 °C for an additional 1 h. The solution was then cooled to room temperature, and 10 mL of methanol was added.

2.3. Device Fabrication. Regioregular (rr) P3HT was purchased from Rieke Metals, and PCBM was purchased from Nano-C. rr-P3HT- and PCBM-based OPV devices were dissolved in *o*-dichlorobenzene (*o*-DCB) in a 1:1 ratio (40 mg total concentration) and stirred overnight at 75 °C. The PCDTBT:$PC_{71}BM$ blend was prepared according to the following procedure: PCDTBT (Solaris Chem.) and $PC_{71}BM$ (Solenne B.V.) (1:4 w/w) were dissolved in a mixture of chlorobenzene (CB) and *o*-DCB (1:3 v/v) and stirred overnight at 70 °C. The devices were fabricated on 20 mm × 15 mm indium-tin-oxide (ITO) glass substrates with sheet resistance of ∼20 Ω/sq. As a hole transport layer, poly(ethylene-dioxythiophene) doped with poly(4-styrenesulfonate) (PEDOT:PSS), purchased from Heraeus (Al 4083), was spin-cast from an aqueous solution on the ITO substrate at 5000 rpm for 30 s (average thickness ≈ 40 nm) for P3HT:PCBM- and at 6000 rpm for 60 s (average thickness ≈ 30 nm) for PCDTBT:$PC_{71}BM$-based devices and was subsequently baked for 15 min at 120 °C in ambient conditions. Following the preparation of the blends, metallic NPs were blended into both solutions in nitrogen saturated atmosphere. To optimize the PV performances, we initially prepared composite blends with different wt % Al NPs for both types of blends; however, those exhibiting the best performance among them were chosen. All hybrid photoactive layers were subsequently deposited by spin-coating the blend solutions at 1000 rpm. In the case of PCDTBT:$PC_{71}BM$-based devices as an electron transport layer, the solution-processed titanium sub oxide (TiO_x) was utilized. The TiO_x interlayer was dissolved in methanol (1:200) and then spin-coated to a thickness of ∼10 nm (6000 rpm, 40 s) in air.[23] The sample was heated at 80 °C for 1 min in air.

Lastly, 100 nm of Al was deposited through a shadow mask by thermal evaporation on the devices through a shadow mask to define an active area of 4 mm^2 for each device. The P3HT:PCBM-based devices were postannealed at 160 °C for 15 min in a glovebox under nitrogen atmosphere. The performances of the devices were measured at room temperature with an Air Mass 1.5 Global (A.M. 1.5 G) solar simulator at an intensity of 100 mW cm^{-2}. A reference monocrystalline silicon solar cell from Newport Corporation was used to calibrate the light intensity. All measurements were made in air immediately after device fabrication without any encapsulation process. The external quantum efficiency measurements were conducted immediately after device fabrication in ambient conditions using an integrated system (Enlitech, Taiwan) and a lock-in amplifier with a current preamplifier under short-circuit conditions. The light spectrum was calibrated using a monocrystalline silicon photodetector of known spectral response. The OPV devices were measured using a Xe lamp passing through a monochromator and an optical chopper at low frequencies (∼200 Hz) to maximize the sound/noise (S/N) ratio.

2.4. Photoluminescence Measurements. For the PL experiments, the devices were placed into a vacuum chamber with optical access. For sample excitation, a He−Cd CW laser operating at a wavelength of 325 nm with 35 mW power was used. The PL spectra were measured at room temperature and resolved using UV grating and a sensitive, calibrated liquid nitrogen-cooled CCD camera. For the PL decay experiments, the samples were initially (t < 0s) illuminated (AM1.5 solar irradiation, 100 mW/cm^2) under vacuum. For t > 0 s, the sample was concurrently exposed to light and air. This led to continuing decay of the PL that was monitored at certain time intervals.

2.5. Laser-Induced Fluorescence (LIF) Experiments. For the LIF experiments, the devices were unencapsulated and exposed to ambient air. They were placed on an X-Y stage. For sample excitation, a Spectron pulsed nanosecond Q-switched Nd:YAG laser, operating at its second harmonic of 532 nm, is used. The duration of every pulse is ∼10 ns, and the energy that was used for the excitation of the devices is ∼40 μJ (fluence 0.4 mJ cm^{-2}). The fluorescence measurements were performed at room temperature and resolved using an Andor Technology Mechelle 5000 spectrograph that is connected to an Andor iStar 734 Series, time-resolved, cooled and intensified charge-

DOI: 10.1021/acsami.5b03970
ACS Appl. Mater. Interfaces 2015, 7, 17756−17764

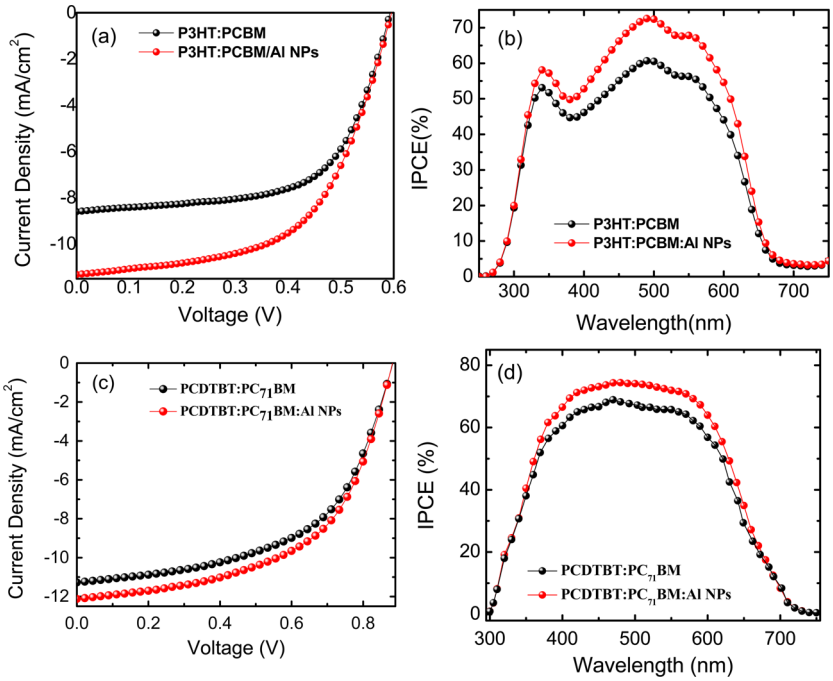

Figure 1. Plot of current density−voltage (J−V) characteristics of reference and Al NP-doped OPV devices using the P3HT:PCBM (a) and PCDTBT:PC$_{71}$BM BHJ blends (c). The corresponding IPCE curves are plotted in (b) and (d), respectively.

Table 1. Electronic Properties of the Reference and Al NP-Doped Devices Defined in the Text

active layer	J_{sc} (mA cm^{-2})	V_{oc} (V)	FF (%)	PCE (%)
P3HT:PCBM	8.60 ± 0.16	0.60	61.17 ± 0.41	3.16 ± 0.08
P3HT:PCBM:Al NPs	11.32 ± 0.21	0.60	60.22 ± 0.53	4.09 ± 0.11
PCDTBT:PC$_{71}$BM	11.29 ± 0.14	0.88	55.13 ± 0.33	5.48 ± 0.10
PCDTBT:PC$_{71}$BM:Al NPs	12.13 ± 0.23	0.88	56.21 ± 0.45	6.00 ± 0.16

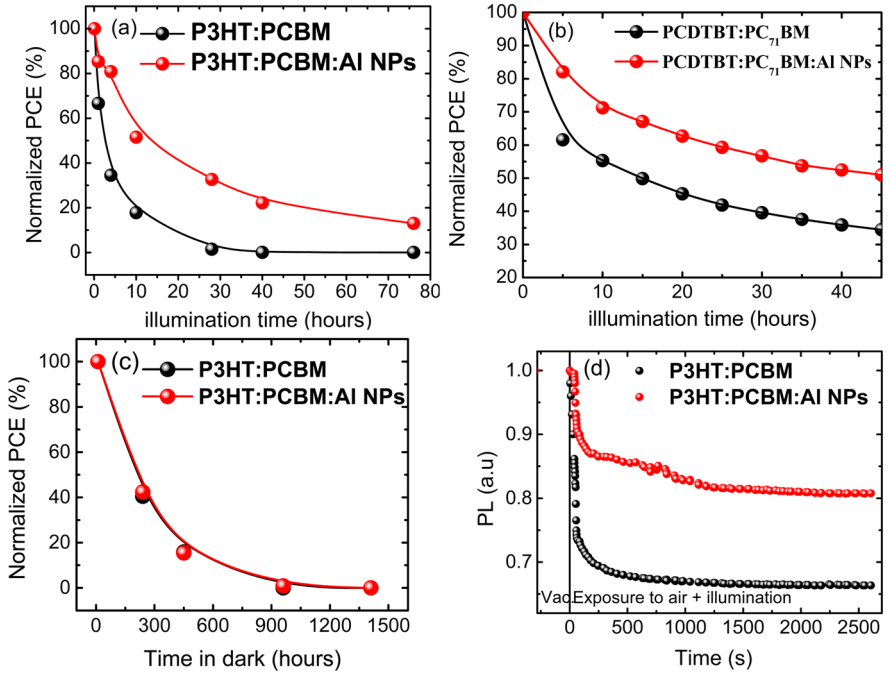

Figure 2. Normalized PCE values vs illumination time for the reference and Al NP-doped OPV devices using the P3HT:PCBM (a) and PCDTBT:PC$_{71}$BM BHJ blends (b). The respective PCE dependence on dark storage time for the P3HT:PCBM-based devices is shown in (c). (d) Photoluminescence decay of reference (black spheres) and Al NP-doped (red spheres) P3HT:PCBM-based devices.

DOI: 10.1021/acsami.5b03970
ACS Appl. Mater. Interfaces 2015, 7, 17756−17764

Scheme 1. Schematic of the Photo-oxidation Process in the Polymer:Al NP Active Layer[a]

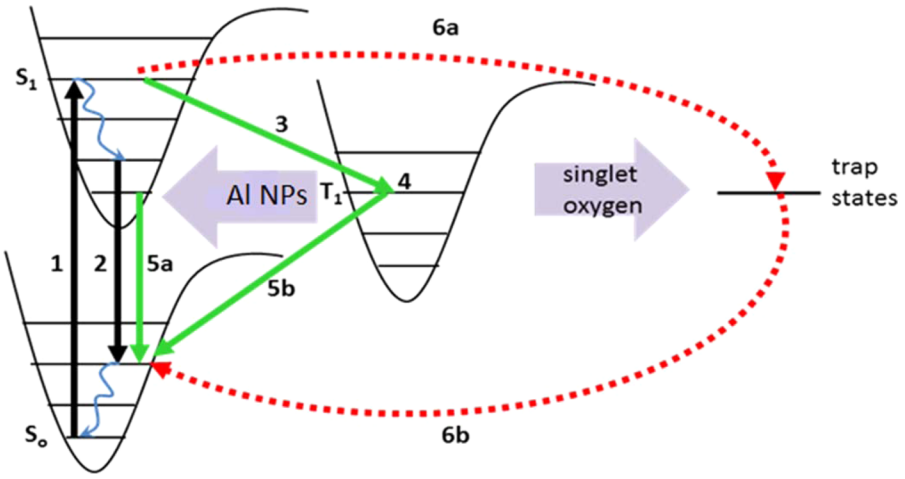

[a]Energy from the polymer triplet excitons excites singlet oxygen, which reacts with the polymer chains to form exciton trap states. The Al NPs embedded into the blend act as quenchers of the triplet excitons, and in this way, the photo-oxidation process can be impeded. 1, absorption; 2, luminescence; 3, system intercrossing; 4, triplet state; 5a, fluorescence; 5b, triplet quenching; and 6a/6b, exciton recombination via trap states. This process is limited in the presence of a triplet quencher.

coupled device (ICCD). For the fluorescence decay experiments, the samples were initially ($t < 0$ s) illuminated (AM 1.5 solar irradiation, 100 mW cm^{-2}) while being exposed to ambient air. For $t > 0$ s, the samples that were used for the study of the fluorescence decay under illumination were concurrently exposed to light and air. The decay is monitored at certain time intervals. For the samples that were stored in the dark, the decay of the fluorescence was also monitored at certain time intervals.

2.6. Fourier Transform Infrared Spectroscopy. FTIR measurements were carried out by means of a Jasco FT/IR 470 Plus interferometer (Italy) equipped with an IRTRON IRT-30 microscope. Each spectrum was acquired in transmittance mode by executing 300 scans at 8 cm^{-1} resolution.

3. RESULTS AND DISCUSSION

Figure 1 displays the illuminated current voltage ($J-V$) characteristics of the reference and Al NP-doped, optimized photovoltaic devices based on two different types of BHJ active layers, i.e., P3HT:PCBM (Figure 1a) and PCDTBT:PCBM (Figure 1b). The respective averaged photovoltaic characteristics are summarized in Table 1. In both cases, the incorporation of Al NPs into the active layer induces a significant improvement in the device short-circuit current (J_{SC}), whereas the open-circuit voltage (V_{OC}) and fill factor (FF) remain almost constant. As a result, the respective PCEs are increased by 29.6 and by 9.5%. We have previously reported that the improved performance of Al NP-doped P3HT:PCBM blend can be attributed to multiple light scattering effects from the large-diameter Al NPs.[11] The observed enhancement in the high-efficiency PCDTBT:PCBM BHJ system as well suggests that doping with Al NPs is a universal and efficient way to enhance the PCE of BHJ OPVs. Following the fabrication and initial measurement of photovoltaic characteristics, the stability of the devices against degradation is measured by performing successive $J-V$ recordings. To simulate outdoor conditions, the degradation experiments were performed with the devices being unencapsulated and exposed to ambient air during operation. The results are presented for two different measurement procedures related to sample storage conditions among measurements. In particular, between two successive $J-V$ recordings, devices were either stored in the dark or continuously illuminated in the open circuit mode. Panels a and b in Figure 2 present the evolution of the respective normalized PCEs (aging curves) over exposure time for the reference and Al NP-doped devices following continuous operation under illumination. For each data point of the curves, a complete $J-V$ characteristic was recorded, and the normalized, J_{sc}, FF, V_{oc}, and PCE values were subsequently calculated. Figure S2 presents the evolution of the J_{sc}, FF, and V_{oc} parameters as well. It is clear that for both BHJ systems, PCE can be better preserved due to the presence of Al NPs. Indeed, for the P3HT:PCBM and P3HT:PCBM:Al NP active layers, 2.5 and 13.5 h of continuous illumination, respectively, are required for a 50% reduction of PCE with respect to its initial value. The situation is similar for the PCDTBT:PC$_{71}$BM and PCDTBT:PCBM:Al NP systems requiring 14.5 and ~45 h, respectively, for the same PCE reduction to be attained. These results indicate that incorporation of Al NPs into the BHJ active layer significantly mitigates performance deterioration due to photodegradation. On the contrary, as indicated in Figure 2c, there is practically no difference in the corresponding PCE evolutions between the reference and Al NP-doped P3HT:PCBM-based devices stored in the dark. Similar observations were made for the device hosting a PCDTBT:PC$_{71}$BM active layer (not shown). It can be concluded that the observed stability enhancement phenomenon takes place only under illumination, suggesting that Al NPs strongly affect the OPV photodegradation pathways,[24] whereas their effect is not related to aging mechanisms occurring in the dark.[25]

To probe the underlying mechanism behind the observed effect of Al NPs against photodegradation, we have proceeded to optical spectroscopy studies of the pristine and doped P3HT:PCBM blends. The reason is that it is the best characterized BHJ system, but more importantly, it is highly reproducible, thus enabling a quantitative spectroscopic study. In a first step, on the basis of the above results, we have considered that the presence of Al NPs may hinder the process behind photoinduced oxidation of the conjugated polymer component in the blend.[26,27,20] As presented in Scheme 1, during photo-oxidation of semiconducting polymers, singlet oxygen formed via energy transfer from the polymer triplet

DOI: 10.1021/acsami.5b03970
ACS Appl. Mater. Interfaces 2015, 7, 17756−17764

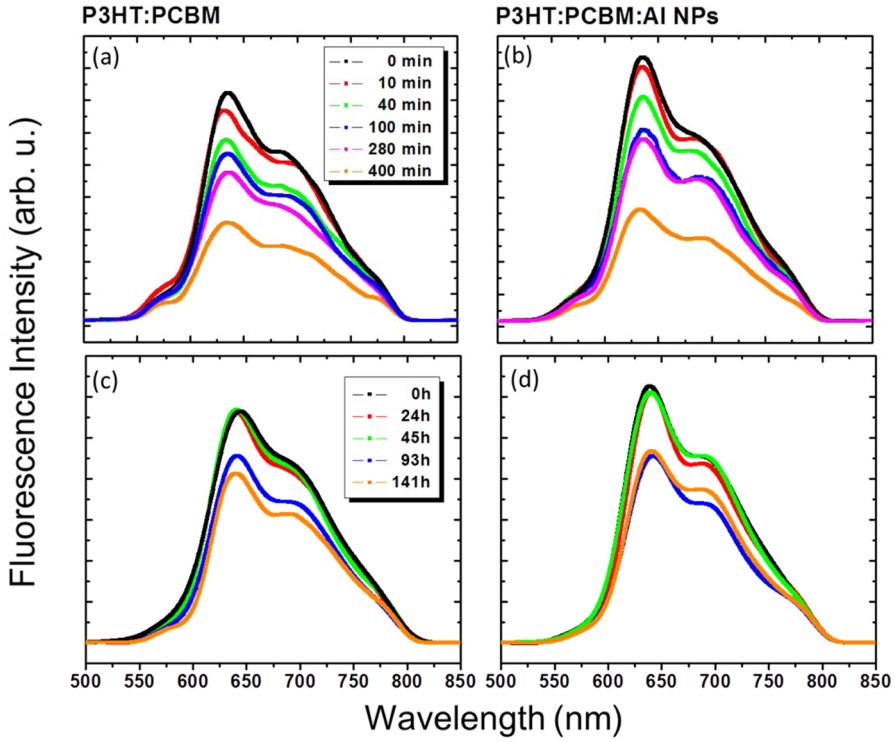

Figure 3. Laser-induced fluorescence spectra of reference (a) and Al NP-doped devices (b) after illumination at certain time intervals shown in the inset and reference (c) and Al NP-doped (d) devices stored in the dark. Excitation wavelength at 532 nm using an Nd:YAG ns laser.

exciton reacts with the polymer to generate exciton traps (paths 6a and 6b in Scheme 1). Such traps are topological defects comprised of carbonyl groups formed on the ends of polymer chains and provide an additional nonradiative channel for the polymer singlet excitons. As a result, quenching of polymer luminescence is induced. In donor:acceptor (D:A) blends, the charge transfer from polymer to fullerene is the dominant process, and therefore, it partially prevents intersystem crossing to a triplet state. Under certain conditions, the formation of triplets in polymer:fullerene blends is also possible as it depends on the relative energy positions of polymer triplet excitons and the fullerene LUMO level.[28] Formed triplet excitons located on the polymer can then nonradiatively relax to the ground state. Additional reactions emerge upon introduction of molecular oxygen, which has a triplet ground state configuration ($^3O_2$). The polymer triplet excitons can undergo energy transfer to the triplet oxygen to generate excited singlet oxygen ($^1O_2$*). It can be concluded that the mechanisms described in Scheme 1 are valid and present in polymer:fullerene blends as well. In the present case, Al NPs may play the role of a stabilizer that blocks the action of oxygen. In particular, as shown in Scheme 1, we postulate that the triplet excitons may be quenched as a result of the overlap of their energy levels with the plasmon resonance of the embedded Al NPs (paths 3, 4, and 5b in Scheme 1).[29]

To investigate this possibility, we performed PL decay measurements, which are a proper means to quantify singlet quenching in P3HT under oxygen exposure. Figure 2d presents the results for the reference compared to the Al NP-doped blend. These measurements correspond to the evolution of the first emission peak values at 635 nm, following laser excitation at 325 nm. It is clear that the addition of NPs into the blend significantly retards its PL intensity decay rate. Indeed, the absorption spectrum of Al NPs in ethanol (Figure S1) comprises a characteristic broad peak corresponding to the NPs' plasmon resonance. This peak is centered at ∼340 nm; however, it is expected to be substantially red-shifted when the NPs are embedded into the higher-refractive index compared to the ethanol polymer matrix.[30] Such a red-shift combined with the broadband nature of NPs' absorption peak may give rise to partial overlap with the triplet excitons band lying in the range 800−1300 nm for both polymer donor systems used in this study.[31] Considering that the NPs resonance has an excitation lifetime of a few picoseconds, the donor-acceptor interaction between the comparatively long-lived triplet excitons of P3HT and the Al NPs will result in strong quenching of the triplet state and thus the photo-oxidation rate. Alternatively, the photoexcited excitons are highly mobile along the conjugated polymer backbone and may hop between chains toward the lowest-energy areas of the film. It is possible that the Al NPs dispersed in the polymer blend will give rise to variations in the local energy environment of the triplet excitons, attracting them toward Al NPs where the triplet exciton-Al NP interaction can easily take place.[26] Specifically, as the size of particles decreases to the nanometer scale, the surface area of the particles increases dramatically, and the NPs act as an effective scavenger of the polymer triplet state.[32]

To further study the degradation process, we additionally performed fluorescence experiments. For this purpose, reference and Al NP-doped devices were submitted to a long-term degradation process in air, and the decay of their fluorescence signal was recorded both under dark storage and during illumination (three pairs of samples for each case). In this way, it was possible to discriminate the aging processes related to light exposure from those due to ambient environment (air) alone. Moreover, we were able to examine the contribution of the Al NPs to the photovoltaic effect and the stability of the device. The collected fluorescence spectra

DOI: 10.1021/acsami.5b03970
ACS Appl. Mater. Interfaces 2015, 7, 17756−17764

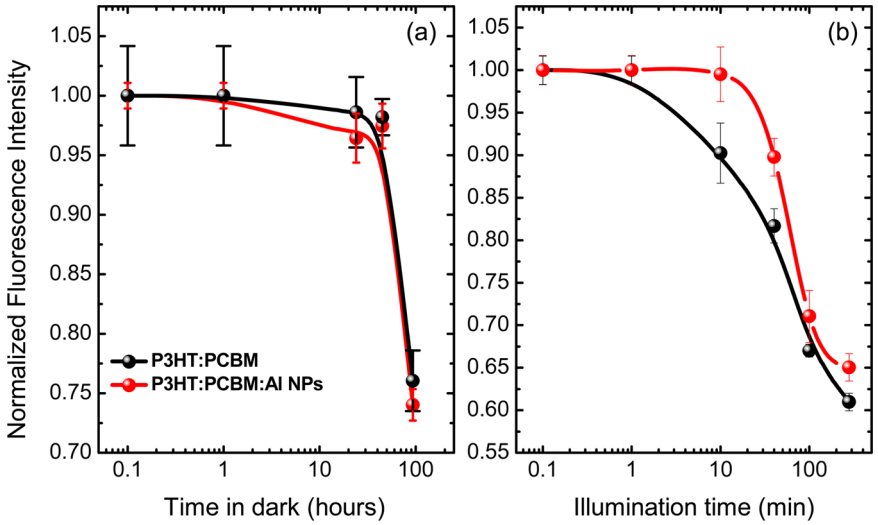

Figure 4. (a) Normalized fluorescence decay of reference and Al NP-doped devices stored in the dark. (b) Normalized fluorescence decay of reference and Al NP-doped devices illuminated at certain time intervals. Excitation wavelength at 532 nm using an Nd:YAG ns laser. The normalized values corresponding to the peak emission wavelength at 635 nm are plotted.

are presented in Figure 3, and Figure 4 compares the normalized fluorescence intensity calculated using the peak values of such spectra at 635 nm, following laser excitation at 532 nm, as a function of the dark storage and illumination times. As can be seen in Figure 4b, the fluorescence signal of the reference device degrades rapidly upon illumination following a first order exponential decay. On the contrary, the Al NP-based device is more stable under illumination, especially in the first 10 h of illumination where the PCE photodegradation rate is significant (Figure 2c). In this case, the fluorescence decay is well fitted by a sigmoidal curve, indicating the fluorescence decay mitigation effect. On the contrary, there is no evidence of any mitigation effect when the same blends are monitored while the samples were stored in the dark in ambient air (Figure 4a). These results are in accordance with the PCE degradation experiments presented in Figure 2 and further confirm the NP-mediated preservation effect of the polymer optical properties evident only under prolonged illumination.

The different dynamics observed for the fluorescence decay signal between light and dark conditions implies the presence of two separate degradation pathways affecting the BHJ system. Our results above suggest that incorporation of Al NPs affects only the pathway under light exposure. To further explore these phenomena, we used FTIR spectroscopy to provide insight on the chemical bonding changes that take place under illumination or dark storage of the reference and Al NP-doped devices.

As shown in Figure 5, the FTIR spectra of the reference and Al NPs devices in their pristine states exhibit remarkable differences. In particular, the reference device shows a broad band at 1530 cm^{-1}, being the convolution of the two resonant quinoidal and benzoic structures of the thiophene ring in PEDOT, which are equally represented in the as-deposited film.[33] This broad band also includes the C═C stretching of P3HT aromatic ring positioned at 1515 cm^{-1}. In the pristine state of the Al NP-doped sample, however, two sharp and distinct bands are evidenced at 1515 and 1548 cm^{-1}. This may be an indication that the Al NPs interfacing the PEDOT:PSS buffer layer could modify the balance between the two resonant structures of PEDOT and consequently its packing structure. Furthermore, the band at 1292−1314 cm^{-1} in the reference sample red-shifts toward 1263 cm^{-1} in the Al NP-doped sample. This region is generally associated with the acyl- or phenol-C−O stretching, corresponding to the ethylene-dioxy group in PEDOT. The red-shift is a further hint of a structural rearrangement occurring in the buffer layer due to Al NP doping. Finally, in the reference sample, the following PSS characteristic bands are visible: asymmetric S−O stretching vibrations at 1120 cm^{-1} and S═O stretching due to the SO_3^- band at 1388 cm^{-1}. These bands are red-shifted toward 1059 and 1330 cm^{-1}, respectively, in the Al NP-doped system. The latter band is a shoulder convolved to the stronger ethylene-dioxy signal. These observations comply with partial Al NP diffusion at the active layer/buffer layer interface, causing modification of the PEDOT:PSS chain motion.

Panels b and c in Figure 5 present the FTIR data for reference and NP-based layers following dark storage for 3 weeks in air. A general observation is that the characteristic band intensities decrease after storage, indicating degradation of the buffer layer. For the reference system, the bands showing the most remarkable modifications will now be discussed. First, there is a red-shift of the C═C stretching thiophene ring vibration from 1530 to 1515 cm^{-1}, with the final value almost approaching the characteristic band of pure P3HT, whereas a less intense band at 1548 cm^{-1} is detected after dark storage. This is an indication that exposure to ambient conditions has modified the balance between the resonant quinoidal and benzoic structures of the thiophene ring in PEDOT, characterizing the as-deposited films. As a result, the (less conductive) benzoic contribution of PEDOT becomes dominant over the quinoidal (conductive) one. An additional spectrum modification is related to the band, including the 1292 and 1314 cm^{-1} modes, red-shifting toward 1270 cm^{-1}. This region is associated with the ethylene-dioxy group in PEDOT, and the red-shift observed implies structural rearrangement occurring during ambient storage. In addition, the PSS characteristic bands at 1118 cm^{-1} (asymmetric S−O stretching vibrations) and at 1388 cm^{-1} (S═O stretching due to SO_3^-) are strongly reduced, indicating that PSS modification occurs upon dark storage, possibly due to ambient moisture (PSS is highly soluble in water). Such degradation may affect the bond

DOI: 10.1021/acsami.5b03970
ACS Appl. Mater. Interfaces 2015, 7, 17756−17764

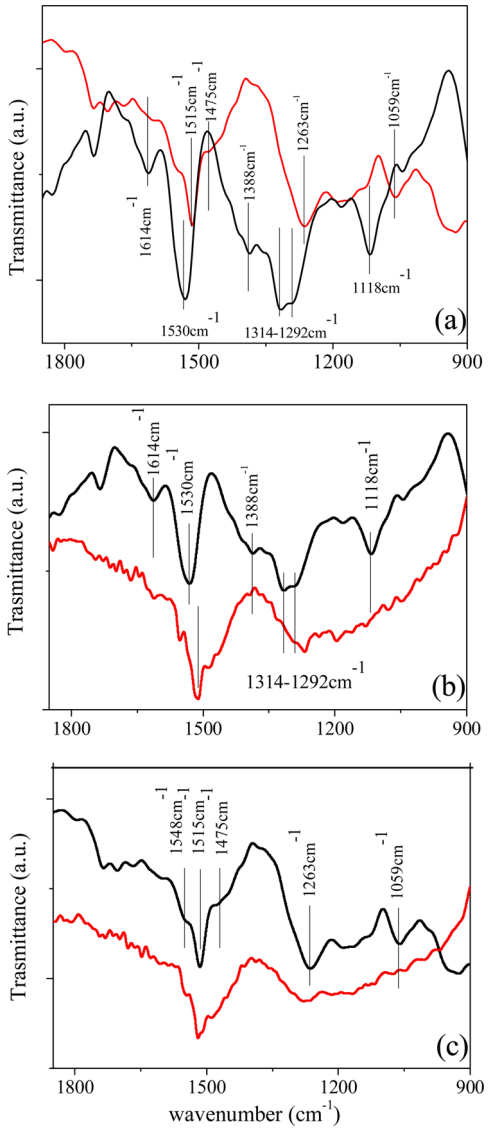

Figure 5. (a) FTIR measurements of pristine samples: reference sample, black line; Al NP sample, red line. FTIR measurements of reference (b) and Al-doped (c) devices: black line, pristine state; red line, dark storage state. The vibrational modes corresponding to the labeled wavenumbers are reported in Table 2.

Table 2. Vibrational Modes Corresponding to the Wavenumbers Labeled in Figures 5 and 6

wavenumber (cm^{-1})	functional group
1059	$-SO_3^-$ sym. stretch
1118	S−O asym. stretch
1190	C−O stretch in esters
1263	red shift of 1292 vibration
1292−1314	C−O stretch ethilendioxy group
1388	S═O stretch
1475	red shift of 1515
1515	C═C sym. stretch in aromatic
1530−1548	tiophene stretch
1614	C═C asym. stretch in aromatic
3550	O−H stretch

between the SOH_3 group and the insulating chains of PSS, inducing a reduced interaction between PEDOT and PSS.

Similar to the reference sample, the band intensities of the FTIR spectrum of the Al NP-doped system decreased after storage (Figure 5c), indicating degradation of both the structure of the PEDOT:PSS and P3HT polymeric components. However, contrary to the reference system, the characteristic peaks of PEDOT and P3HT were not shifted. The only remarkable effect is the suppression of the PSS characteristic bands at 1059 and 1263 cm^{-1}, suggesting that the contribution to buffer layer degradation is limited to its hygroscopic component as a consequence of exposure to ambient moisture.

The comparison of the FTIR spectra of the reference sample in its pristine relative to illuminated state, presented in Figure 6,

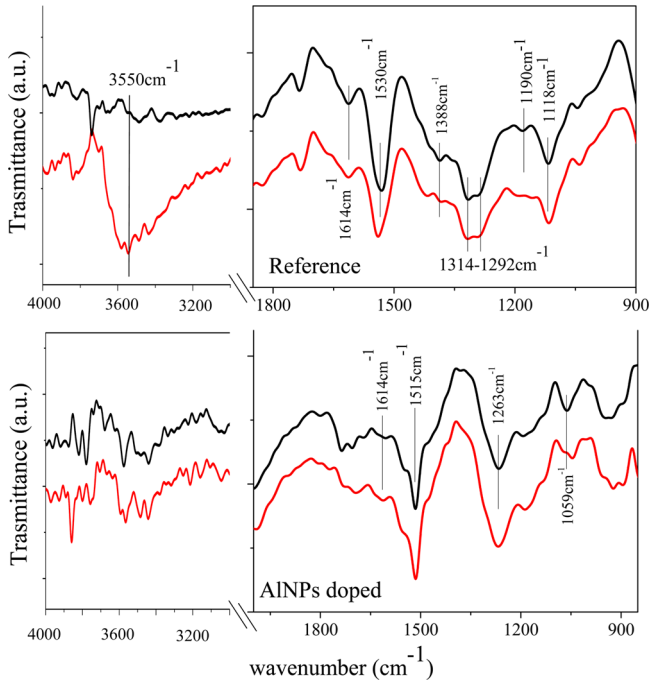

Figure 6. FTIR measurements of reference (top) and Al-doped devices (bottom): black line, pristine state; red line, illuminated state. The vibrational modes corresponding to the labeled wavenumbers are reported in Table 2.

does not provide evidence of any shift of the buffer layer vibrational bands, indicating that the PEDOT:PSS layer remains stable upon light exposure. However, there is a prominent decrease in the 1530 cm^{-1} peak intensity attributed to both PEDOT and P3HT. However, because no variation was observed for the rest of the PEDOT and PSS vibrational modes, we may assume that the 1530 cm^{-1} intensity loss is a fingerprint of P3HT photo-oxidation as previously reported in the literature.[34] Further information on the BHJ degradation under light exposure can also be deduced from the strong reduction of the band at 1190 cm^{-1} related to C−C−O stretching in PCBM. This suggests that illumination may favor diffusion of the water molecules into the BHJ and that PCBM ester hydrolysis occurs spontaneously.[35] This is also confirmed by the appearance of the broad band at 3550 cm^{-1} (inset of Figure 6a), which is the spectral marker of the stretching mode of (OH) groups (with alcohol being the secondary product of the ester hydrolysis). On the contrary, the FTIR bands of the NP-doped system remain unchanged after prolonged illumination. Only a band intensity decrease was observed, indicating a

DOI: 10.1021/acsami.5b03970
ACS Appl. Mater. Interfaces 2015, 7, 17756−17764

general degradation of the structure of the PEDOT:PSS and P3HT polymeric components. These data suggest that no structural modifications occur in the Al NP-doped system upon prolonged illumination.

Summarizing the FTIR results, we can state that the following aging processes are evidenced under dark storage of the reference sample: PEDOT degradation (favoring a less conductive structure) and PSS modification. The former process is inhibited when Al NPs are introduced in the BHJ and only PSS modification, related to its hygroscopic nature, persists. This effect may be due to the presence of some Al NPs in contact with the hole transporting layer, which may hinder the PEDOT:PSS chain motions, leading to an effective increase of the conformational stability. It should be mentioned here that the identical dark lifetime degradation measured for both types of cells, namely, reference and Al NP-doped, indicates that the dark IV characteristics may not be sensitive to such changes in the PEDOT:PSS structure. This is in accordance with the literature, stating that the dark current is typically not a figure of merit in solar cell devices.[36] Conversely, all aging processes evidenced in the reference sample under illumination are inhibited upon incorporation of Al NPs into the BHJ blend.

The FTIR results complemented with the PL and fluorescence studies presented above provide us with important information on the different degradation pathways occurring upon illumination. In particular, our results show that P3HT photo-oxidation, which is the primary pathway, is significantly mitigated in the Al NP-doped OPV cells, possibly due to the fact that Al NPs function as triplet quenchers (Scheme 1). Besides this, a second degradation pathway present upon illumination is related to PCBM hydrolysis, which gives rise to the creation of trap states acting as fluorescence quenchers, which thus influence exciton generation. We postulate that solar illumination could mediate the formation of an aluminum-oxide (Al_2O_3) coating on the NP surface. In particular, due to exposure to air and moisture conditions, water molecules diffusing in the BHJ will react under illumination with the NPs surface, leading to Al_2O_3 corrosion, which is well-known as a spontaneous reaction process.[37] Such a process is facilitated by the absence of any surfactant coating on the Al NP surface[38,39] because the NPs used here were produced by a physical synthetic method. As a result of this process, the availability of water molecules promoting PCBM hydrolysis is limited. Finally the third aging process identified by FTIR analysis is associated with degradation of the PEDOT:PSS layer. This aging pathway is always present upon exposure to air, whereas the presence of Al NPs at the active layer/buffer layer interface partially influences the PEDOT:PSS chain motion.

4. CONCLUSIONS

We have reported on a remarkable enhancement of an OPV device's lifetime upon incorporation of Al NPs into the BHJ active layer. This significant improvement in stability of the devices is presented for two different, widely used BHJ systems. FTIR complemented with PL and fluorescence spectroscopy measurements revealed the mitigation of two different photodegradation pathways attributed to the presence of Al NPs. First, NP incorporation blocks the polymer donor photo-oxidation via the oxygen-assisted formation of triplet excitons, possibly due the overlap of such excitonic levels with the plasmon resonance of the embedded Al NPs. Second, it inhibits PCBM hydrolysis, possibly due to the light-mediated corrosive reaction with water molecules leading to Al_2O_3 surface layer formation. This work proposes the application of Al NP-doping as an efficient way to enhance the lifetime of other types of polymer devices as well, including light emitting diodes, detectors, and sensors.

■ ASSOCIATED CONTENT

Supporting Information

The Supporting Information is available free of charge on the ACS Publications website at DOI: 10.1021/acsami.5b03970.

TEM image and size distribution of the fabricated Al nanoparticles and PCE, *J*sc, and FF changes over time with and/or without solar illumination for P3HT:PCBM- and PCDTBT:PC71BM-based OPV devices. (PDF)

■ AUTHOR INFORMATION

Corresponding Authors

*Tel: barbara.paci@ism.cnr.it.

*Tel: 2810-391274, E-mail: stratak@iesl.forth.gr.

Notes

The authors declare no competing financial interest.

■ ACKNOWLEDGMENTS

The authors are grateful for the support received from the COST Action HINT (MP1202). The authors acknowledge M. Guaragno for his support with FTIR experiments. This research has been financially supported by the PeNElOPe (3116) project which is implemented under the ARISTEIA II Action of the Operational Programme Education and Life-long Learning and is co-funded by the European Social Fund (ESF) and National Resources.

■ REFERENCES

(1) Huo, L.; Liu, T.; Sun, X.; Cai, Y.; Heeger, A. J.; Sun, Y. Single-Junction Organic Solar Cells Based on a Novel Wide-Bandgap Polymer with Efficiency of 9.7%. *Adv. Mater.* **2015**, *27*, 2938.

(2) Kong, J.; Hwang, I.-W.; Lee, K. Top-Down Approach for Nanophase Reconstruction in Bulk Heterojunction Solar Cells. *Adv. Mater.* **2014**, *26*, 6275−6283.

(3) Chen, C.-C.; Chang, W.-H.; Yoshimura, K.; Ohya, K.; You, J.; Gao, J.; Hong, Z.; Yang, Y. An Efficient Triple-Junction Polymer Solar Cell Having a Power Conversion Efficiency Exceeding 11%. *Adv. Mater.* **2014**, *26*, 5670−5677.

(4) Gan, Q.; Bartoli, F. J.; Kafafi, Z. H. Plasmonic-Enhanced Organic Photovoltaics: Breaking the 10% Efficiency Barrier. *Adv. Mater.* **2013**, *25*, 2385−2396.

(5) Stratakis, E.; Kymakis, E. Nanoparticles-Based Plasmonic Organic Photovoltaic Devices. *Mater. Today* **2013**, *16*, 133−146.

(6) Wang, C. C. D.; Choy, W. C. H.; Duan, C.; Fung, D. D. S.; Sha, W. E. I.; Xie, F.-X.; Huang, F.; Cao, Y. Optical and Electrical Effects of Gold Nanoparticles in the Active Layer of Polymer Solar Cells. *J. Mater. Chem.* **2012**, *22*, 1206.

(7) Spyropoulos, G. D.; Stylianakis, M. M.; Stratakis, E.; Kymakis, E. Organic Bulk Heterojunction Photovoltaic Devices with Surfactant-Free Au Nanoparticles Embedded in the Active Layer. *Appl. Phys. Lett.* **2012**, *100*, 213904.

(8) Lu, L.; Luo, Z.; Xu, T.; Yu, L. Cooperative Plasmonic Effect of Ag and Au Nanoparticles on Enhancing Performance of Polymer Solar Cells. *Nano Lett.* **2013**, *13*, 59−64.

(9) Li, X.; Choy, W. C. H.; Lu, H.; Sha, W. E. I.; Ho, A. H. P. Efficiency Enhancement of Organic Solar Cells by Using Shape-Dependent Broadband Plasmonic Absorption in Metallic Nanoparticles. *Adv. Funct. Mater.* **2013**, *23*, 2728−2735.

(10) Baek, S.-W.; Noh, J.; Lee, C.-H.; Kim, B.; Seo, M.-K.; Lee, J.-Y. Plasmonic Forward Scattering Effect in Organic Solar Cells: A Powerful Optical Engineering Method. *Sci. Rep.* **2013**, *3*, 1726.

DOI: 10.1021/acsami.5b03970
ACS Appl. Mater. Interfaces 2015, 7, 17756−17764

(11) Kakavelakis, G.; Stratakis, E.; Kymakis, E. Aluminum Nanoparticles for Efficient and Stable Organic Photovoltaics. *RSC Adv.* **2013**, *3*, 16288−16291.
(12) Sha, W. E. I.; Choy, W. C. H.; Liu, Y. G.; Chew, W. C. Near-field Multiple Scattering Effects of Plasmonic Nanospheres Embedded into Thin-film Organic Solar Cells. *Appl. Phys. Lett.* **2011**, *99*, 113304.
(13) Li, X.; Choy, W. C. H; Huo, L.; Xie, F.; Sha, W. E. I.; Ding, B.; Guo, X.; Li, Y.; Hou, J.; You, J.; Yang, Y. Dual Plasmonic Nanostructures for High Performance Inverted Organic Solar Cells. *Adv. Mater.* **2012**, *24*, 3046−3052.
(14) Kakavelakis, G.; Stratakis, E.; Kymakis, E. Synergetic Plasmonic Effect of Al and Au Nanoparticles for Efficiency Enhancement of Air Processed Organic Photovoltaic Devices. *Chem. Commun.* **2014**, *50*, 5285−5287.
(15) Liao, W. P.; Su, Y. H.; Huang, Y. K.; Yeh, C. S.; Huang, L. W.; Wu, J. J. P3HT-Based Nanoarchitectural Fano Solar Cells. *ACS Appl. Mater. Interfaces* **2014**, *6*, 17993−18000.
(16) Choy, W. C. H. The Emerging Multiple Metal Nanostructures for Enhancing the Light Trapping of Thin Film Organic Photovoltaic Cells. *Chem. Commun.* **2014**, *50*, 11984−11993.
(17) Paci, B.; Spyropoulos, G. D.; Generosi, A.; Bailo, D.; Albertini, V. R.; Stratakis, E.; Kymakis, E. Enhanced Structural Stability and Performance Durability of Bulk Heterojunction Photovoltaic Devices Incorporating Metallic Nanoparticles. *Adv. Funct. Mater.* **2011**, *21*, 3573−3582.
(18) Reese, M. O.; Nardes, A. M.; Rupert, B. L.; Larsen, R. E.; Olson, D. C.; Lloyd, M. T.; Shaheen, S. E.; Ginley, D. S.; Rumbles, G.; Kopidakis, N. Photoinduced Degradation of Polymer and Polymer−Fullerene Active Layers: Experiment and Theory. *Adv. Funct. Mater.* **2010**, *20*, 3476−3483.
(19) Reese, M. O.; Morfa, A. J.; White, M. S.; Kopidakis, N.; Shaheen, S. E.; Rumbles, G.; Ginley, D. Pathways for the Degradation of Organic Photovoltaic P3HT: PCBM Based Devices. *Sol. Energy Mater. Sol. Cells* **2008**, *92*, 746−752.
(20) Paci, B.; Generosi, A.; Albertini, V. R.; Spyropoulos, G. D.; Stratakis, E.; Kymakis, E. Enhancement of Photo/Thermal Stability of Organic Bulk Heterojunction Photovoltaic Devices via Gold Nanoparticles Doping of the Active Layer. *Nanoscale* **2012**, *4*, 7452−7459.
(21) Paci, B.; Bailo, D.; Albertini, V. R.; Wright, J.; Ferrero, C.; Spyropoulos, G. D.; Stratakis, E.; Kymakis, E. Spatially-Resolved In-Situ Structural Study of Organic Electronic Devices with Nanoscale Resolution: The Plasmonic Photovoltaic Case Study. *Adv. Mater.* **2013**, *25*, 4760−4765.
(22) Stratakis, E.; Barberoglou, M.; Fotakis, C.; Viau, G.; Garcia, C.; Shafeev, G. A. Generation of Al Nanoparticles via Ablation of Bulk Al in Liquids with Short Laser Pulses. *Opt. Express* **2009**, *17*, 12650−12659.
(23) Kakavelakis, G.; Konios, D.; Stratakis, E.; Kymakis, E. Enhancement of the Efficiency and Stability of Organic Photovoltaic Devices via the Addition of a Lithium-Neutralized Graphene Oxide Electron-Transporting Layer. *Chem. Mater.* **2014**, *26*, 5988−5993.
(24) Paci, B.; Generosi, A.; Rossi Albertini, V.; Perfetti, P.; de Bettignies, R. The Role of C60 Barrier Layer in Improving the Performances of Efficient Polymer-Based Photovoltaic Devices: An AFM/EDXR Time-Resolved Study. *J. Phys. Chem. C* **2009**, *113*, 19740.
(25) Grossiord, N.; Kroon, J.; Andriessen, R.; Blom, P. Degradation Mechanisms in Organic Photovoltaic Devices. *Org. Electron.* **2012**, *13*, 432−456.
(26) Lim, Y. T.; Lee, T.-W.; Lee, H.-C.; Park, O. O. Impediment of Photo-Oxidation in PPV Nanocomposites Doped by Metal Coated Silica Nanoparticles. *Synth. Met.* **2002**, *128*, 133−137.
(27) Park, J. H.; Lim, Y. T.; Park, O. O.; Kyeong Kim, J.; Yu, J.-W.; Kim, Y. C. Polymer/Gold Nanoparticle Nanocomposite Light-Emitting Diodes: Enhancement of Electroluminescence Stability and Quantum Efficiency of Blue-Light-Emitting Polymers. *Chem. Mater.* **2004**, *16*, 688−692.
(28) Sperlich, A.; Kraus, H.; Deibel, C.; Blok, H.; Schmidt, J.; Dyakonov, V. Reversible and Irreversible Interactions of Poly(3-hexylthiophene) with Oxygen Studied by Spin-Sensitive Methods. *J. Phys. Chem. B* **2011**, *115*, 13513−13518.
(29) Roldan, A.; Ricart, J. M.; Illas, F. Origin of the Size Dependence of Au Nanoparticles toward Molecular Oxygen Dissociation. *Theor. Chem. Acc.* **2011**, *128*, 675−681.
(30) Malinsky, M. D.; Kelly, K. L.; Schatz, G. C.; Van Duyne, R. P. Chain Length Dependence and Sensing Capabilities of the Localized Surface Plasmon Resonance of Silver Nanoparticles Chemically Modified with Alkanethiol Self-Assembled Monolayers. *J. Am. Chem. Soc.* **2001**, *123*, 1471−1482.
(31) Etzold, F.; Howard, I. A.; Mauer, R.; Meister, M.; Kim, T. D.; Lee, K. S.; Baek, N. S.; Laquai, F. Ultrafast Exciton Dissociation Followed by Nongeminate Charge Recombination in PCDTBT:PCBM Photovoltaic Blends. *J. Am. Chem. Soc.* **2011**, *133*, 9469−9479.
(32) Park, J. H.; Lim, Y. T.; Park, O. O.; Kim, Y. C. Enhancement of Photostability in Blue-Light-Emitting Polymers Doped with Gold Nanoparticles. *Macromol. Rapid Commun.* **2003**, *24*, 331.
(33) Ouyang, J.; Xu, O.; Chu, C.-W.; Yang, Y.; Li, G.; Shinar, J. On the Mechanism of Conductivity Enhancement in Poly(3,4-ethylenedioxythiophene):Poly(styrene sulfonate) Film through Solvent Treatment. *Polymer* **2004**, *45*, 8443−8450.
(34) Manceau, M.; Chambon, S.; Rivaton, A.; Gardette, J.-L.; Guillerez, S.; Lemaître, N. Effects of Long-Term UV−Visible Light Irradiation in the Absence of Oxygen on P3HT and P3HT: PCBM Blend. *Sol. Energy Mater. Sol. Cells* **2010**, *94*, 1572−1577.
(35) Paci, B.; Generosi, A.; Bailo, D.; Rossi Albertini, V.; de Bettignies, R. Discriminating Bulk, Surface and Interface Aging Effects in Polymer-Based Active Materials for Efficient Photovoltaic Devices. *Chem. Phys. Lett.* **2010**, *494*, 69−74.
(36) Baeg, K.-J.; Binda, M.; Natali, D.; Caironi, M.; Noh, Y.-Y. *Adv. Mater.* **2013**, *25*, 4267.
(37) Li, Y.; Song, W.; Xie, C.; Zeng, D.; Wang, A.; Hu, M. Influence of Humidity on the Thermal Behavior of Aluminum Nanopowders. *Mater. Chem. Phys.* **2006**, *97*, 127−131.
(38) Nishimura, T.; Raman, V. Corrosion Prevention of Aluminum Nanoparticles by Polyurethane Coating. *Materials* **2014**, *7*, 4710−4722.
(39) Shahravan, A.; Desai, T.; Matsoukas, T. Passivation of Aluminum Nanoparticles by Plasma-Enhanced Chemical Vapor Deposition for Energetic Nanomaterials. *ACS Appl. Mater. Interfaces* **2014**, *6* (10), 7942−7947.

DOI: 10.1021/acsami.5b03970
ACS Appl. Mater. Interfaces 2015, 7, 17756−17764